Correlating weathered, microphenocryst-rich, intermediate tephra

Pearce, Nick; Alloway, Brent V.; Wickham, Craig

Published in:
Quaternary International

DOI:
10.1016/j.quaint.2019.01.017

Publication date:
2019

Citation for published version (APA):
Pearce, N., Alloway, B. V., & Wickham, C. (2019). Correlating weathered, microphenocryst-rich, intermediate tephra: An approach combining bulk and single shard analyses from the Lepué Tephra, Chile and Argentina. *Quaternary International*, *500*, 71-82. https://doi.org/10.1016/j.quaint.2019.01.017

Accepted Manuscript

Correlating weathered, microphenocryst-rich, intermediate tephra: An approach combining bulk and single shard analyses from the Lepué Tephra, Chile and Argentina

Nicholas J.G. Pearce, Brent V. Alloway, Craig Wickham

PII: S1040-6182(18)31087-5

DOI: https://doi.org/10.1016/j.quaint.2019.01.017

Reference: JQI 7714

To appear in: *Quaternary International*

Received Date: 26 September 2018

Revised Date: 12 January 2019

Accepted Date: 13 January 2019

Please cite this article as: Pearce, N.J.G., Alloway, B.V., Wickham, C., Correlating weathered, microphenocryst-rich, intermediate tephra: An approach combining bulk and single shard analyses from the Lepué Tephra, Chile and Argentina, *Quaternary International* (2019), doi: https://doi.org/10.1016/j.quaint.2019.01.017.

Correlating weathered, microphenocryst-rich, intermediate tephra: an approach combining bulk and single shard analyses from the Lepué Tephra, Chile and Argentina.

Nicholas J.G. Pearce[1, *], Brent V. Alloway[2,3], Craig Wickham[1,4]

1. Department of Geography & Earth Sciences, Aberystwyth University, SY23 3DB, Wales, UK

2. School of Environment, University of Auckland, Private Bag 92019, Auckland, New Zealand

3. Centre for Archaeological Science (CAS), School of Earth and Environmental Sciences, University of Wollongong, NSW 2522, Australia

4. Present address: SRK Consulting, Churchill Way, Cardiff, CF10 2HH, Wales, UK

*Corresponding author: Nick.Pearce@aber.ac.uk

Submission for the Quaternary International "500" volume

Abstract.

Chemical correlation of intermediate tephra deposits using microanalytical data is problematic because (i) the phenocryst content of their component glass shards affects major and trace element analyses (ii) bulk chemistry can be affected by variations in mineral/lithic components across the fall-out, and (iii) weathering readily alters their composition. All of these problems affect the Lepué Tephra, a prominent marker horizon extensively distributed across the Los Lagos Region of Chile and the Chile-Argentina frontier in north-western Patagonia, which was erupted from Volcán Michinmahuida at *c*. 11000 cal a BP. Weathering of terrestrial cover-bed deposits in this hyper-humid depositional environment leaves only a few occurrences of the tephra which contain fresh glass shards for microbeam analysis, but their highly phenocrystic nature makes data interpretation difficult. Equally, leaching of mobile elements during weathering causes considerable compositional changes across the fall-out region and is evident in bulk sample analyses. Elements such as the REE and Y, generally regarded as immobile, show marked mobility. Within the REE, the development of "M-type" tetrad effects and positive Ce-anomalies result from a combination of dissolution/leaching of the REE from the bulk sample and retention by co-precipitation of Ce^{4+} on Fe-oxyhydroxides in this high-rainfall, hyper-humid, oxic environment. Chemical correlation of the Lepué Tephra is thus not straightforward. However, by careful consideration of the data for a limited range of elements, chemical correlation can be achieved using elements which (i) are incompatible in magmatic systems (and thus their ratios are unaffected by the presence of phenocrysts in single glass shard microbeam analysis) and (ii) are not mobilised in these weathering conditions. These elements are Zr, Hf, Nb, Ta and Th. Their ratios (i) allow for the comparison of single grain and bulk sample analyses, extending the geographic range over which data can be compared for the Lepué Tephra, (ii) provide a robust

chemical correlation of this weathered, intermediate tephra deposit, enabling correlation even where elements traditionally considered immobile (REE, Y, and U) have been significantly mobilised, and (iii) allow the Lepué Tephra to be distinguished from other local tephra deposits. This combined analytical approach enables tephras that have been variably weathered to become useful marker beds over much wider geographical areas than previously feasible, thereby enhancing their tephrochronological application in Quaternary research.

Keywords.

Lepué Tephra; tephrochronology; tephra correlation; REE geochemistry; REE tetrad effect; immobile elements; incompatible elements

1. Introduction

Correlation of intermediate tephra deposits using compositional data can be highly problematic because of the phenocrystic nature of the magma, compositional variation in the magma erupted from zoned magma chambers, and because these intermediate bulk compositions can alter rapidly, whereby the glass phase analyses can be compromised (Alloway et al., 1995; Riehle et al., 1999; Shane, 2005; Donoghue et al., 2007; Lowe et al., 2008). In part for these reasons andesitic tephra have often been overlooked in favour of compositional correlation studies which suffer less from these issues, e.g. using rhyolitic tephra which are often more widespread, or basaltic tephra, often less widespread but erupted frequently in areas such as the North Atlantic from Iceland (Abbott et al., 2013). Specifically, single glass shard analyses by micro-beam methods for major and trace elements of intermediate tephra (i.e. basaltic-andesite and andesite) are often hampered by the presence of abundant phenocrysts which can contribute to the analysis of a “glass” shard (Platz et al., 2007; Lowe, 2011). This phenocryst effect is especially problematic in laser ablation (LA) ICP-MS analysis, where the analysed volume is much greater than in electron probe microanalysis (EPMA). Any analysed material from phenocrystic shards with a “bulk” intermediate composition is highly likely to include phenocrysts, notably plagioclase, which adds Ca and Sr to the analysed material and dilutes the concentration of incompatible elements from the glass phase, which may be dacitic or rhyolitic in composition. These incompatible elements are often very useful in tephra correlation (Pearce et al., 2002; Pearce et al., 2004; Pearce et al., 2007; Pearce et al., 2011; Pearce, 2014; Pearce et al., 2014). Bulk analyses of intermediate tephra, however, can be useful in that they overcome the problem of analysis of variable quantities of phenocrysts with grain-specific methods, but bulk analyses can incorporate xenolithic/xenocrystic material from the eruption, or enclosing sediment intermixed during deposition, and thus require careful sampling. To further complicate their

correlation, bulk tephra composition may change with distance from the vent because of sedimentary fractionation of the erupted material (Sarna-Wojcicki et al., 1981; Juvigné and Porter, 1985). Additionally, intermediate (andesitic) tephra weathers comparatively rapidly (Kirkman and McHardy, 1980; Parfitt et al., 1983; Alloway et al., 1995; Churchman and Lowe, 2012) and consequently analysis and correlation may be further hindered by processes occurring in the soil-forming environment (Cronin et al., 1996; McHenry et al., 2008; Lowe, 2011; Lowe et al., 2017). These factors make the direct comparison of bulk and single grain analyses difficult because of the effect mixing variable proportions of glass with phenocrysts during microbeam analysis can have on single grain data, as well as other compositional effects from lithics or contaminant phases. However, when chosen with care, the use of appropriate element ratios can overcome some of these issues (Pearce et al., 2002; Pearce et al., 2004; Lowe et al., 2017; Martin-Jones et al., 2017b). Here, data from the Lepué Tephra, deposited from a large, early Holocene eruption of Volcán Michinmahuida in the Andean Southern Volcanic Zone of Chile, is used to illustrate several of these problems, and to show how, despite significant challenges related to the physical properties of this deposit, chemical correlation can be achieved in the most unfavourable (analytical and geochemical) conditions. This approach may offer a method for correlation of proximal to distal deposits where preservation varies, and where alteration has affected the concentrations of elements which are generally considered to be immobile (e.g. the rare earth elements, REE). These findings therefore provide a new way of making use of some tephra deposits which were previously considered to have limited value as chronostratigraphic units, making them valuable marker beds over much wider geographical areas, thereby enhancing their potential application to linking and dating deposits and landscapes (i.e. tephrochronologically) in a range of associated Quaternary studies.

2. Lepué Tephra: an introduction

The Lepué Tephra, a prominent marker horizon described in detail by Alloway et al. (2017a), is extensively distributed across the Los Lagos Region of Chile, and straddles the Chile-Argentina frontier in northwest Patagonia (Figure 1). The Lepué Tephra can be correlated to an equivalent-aged >40 m thick pyroclastic flow deposit (Amarillo Ignimbrite) which is well exposed on the south-eastern flanks of Michinmahuida. The source vent or vents of these co-eruptive units (Amarillo Ignimbrite and Lepué Tephra) is/are currently obscured by an extensive ice field which mantles the Michinmahuida volcanic massif, an ice sheet which will have been considerably larger at the time of this eruption.

Figure 1 about here

The Lepué Tephra is well constrained at *c*. 11000 cal a BP from ^{14}C dates from lake and soil cover-bed sequences in the area (Alloway et al., 2017a), where it occurs as a deposit ranging from less than a centimetre in thickness to the north of Lago Llanquihue, a few centimetres to a decimetre thick on Isla Grande de Chiloé or in the vicinity of Puerto Montt, and up to (and more than) ~ 2 m in thickness near the town of Chaitén to the immediate WSW of Volcán Michinmahuida. Lake cores from across the region record between 2 cm to 28 cm of Lepué Tephra, and ODP core 1233D (Leg 202) (Tiedemann et al., 2007) contains 12 cm of the tephra, ~260 km NW of Volcán Michinmahuida. The Lepué Tephra is almost invariably the lowest tephra observed stratigraphically in the post-glacial cover-bed sequence in this area, closely overlying either glacial till/diamicton deposits from the Last Glacial Maximum or local bedrock. Figure 2 illustrates the range of field occurrences from proximal to distal of the Lepué Tephra throughout northwest Patagonia. Lepué Tephra underlies the Chana Tephra (previously referred to as Cha-1, Naranjo and Stern, 2004), the ~9.7 ka eruption of Volcán Chaitén (see Figure 2F), although several intensely weathered scoriaceous lapilli tephra deposits from other local volcanoes (presumably Volcánes Corcovado, Yate or Calbuco, see Figure 2C) may intervene but these are as yet uncharacterised (Alloway et al., 2017b).

Figure 2 about here

The Lepué Tephra has many characteristics typical of a phreatomagmatic eruptive from a compositionally zoned magma body, and produces a complex and variable tephra deposit (Figure 2A). In sections close to Volcán Michinmahuida, proximal Lepué Tephra is typically a compact, dark grey to brownish-grey, poorly sorted, massive to weakly stratified, scoriaceous lapilli to lapilli-tuff (i.e. a consolidated lapilli tuff) of basaltic–andesitic bulk composition which often contains accretionary lapilli up to ~3 cm in diameter (Figure 2B). This sometimes overlies a prominent decimetre-thick red-brown medium-coarse (lapilli-size) scoriaceous fall unit from a magmatic phase of the same eruption (Figure 2A). The combination of these textural features and variable sorting of the deposit suggested to Alloway et al. (2017a) that variable interaction with significant quantities of water during the eruption (Zimanowski, 2001) resulted in a complex intermixing of magmatic and phreatomagmatic eruptive components (Cas and Wright, 1987), with the water here largely derived from melting of the overlying ice cap. In places close to the source, the typical, massive accretionary lapilli-tuff overlies a basal rhyolitic ash and a surge unit containing moderately sorted, inclined planar to low-angle cross-bedded, scoriaceous ash and lapilli beds (not illustrated here, but see Alloway et al., 2017a). At intermediate distances (between ~30 km to 60 km from Volcán Michinmahuida), the Lepué Tephra is between ~30 cm to 100 cm in thickness and typically is characterized by a decimetre-thick weakly stratified, brownish grey, very poorly sorted cemented ash with indistinct centimetre-sized accretionary lapilli and scoriaceous lapilli-rich ashy intra-beds (Figures 2B and 2C).

Distally, >~60 km to 100 km from the source, the Lepué Tephra is deposited across much of Isla Grande de Chiloé and its adjacent islands and the area around Puerto Montt (Figures 2D, 2E, 2F). In Chiloé the Lepué Tephra is the only macroscopic tephra that can be observed within the late last glacial/post-glacial andic soil cover-beds, where it occurs as laterally discontinuous cemented aggregates of olive-brown to reddish-brown fine to medium ash, and it typically closely overlies late last glacial to Last Glacial Maximum (LGM)-aged colluvium, fluvio-glacial gravels and sands, and glacial diamicts (till) (Figure 2E). Across this distal fallout region, the Lepué Tephra can be hard to observe within the andic (allophane- and ferrihydrite-rich) soil cover-beds as it forms highly irregular, discontinuous pods of crudely bedded, cemented fine- to medium-ash enveloped by similarly reddish-brown andic soil material (Figures 2E, 2F). This similarity with its enclosing sediments allowed its distal extent to remain unrecognised in previous studies in the area (Naranjo and Stern, 2004; Watt et al., 2011). Further details of the stratigraphic context and variations within the Lepué Tephra, along with details of all localities sampled for analysis in this study are given by Alloway et al. (2017a), which should be consulted for details of the eruption and deposition history, and major element chemical variation of the deposit, which are not reiterated here.

3. Sampling and analytical data.

The Lepué Tephra was sampled extensively for chemical and mineralogical analysis of both bulk material and single glass shards, across its visible fallout range and also from lake and ODP core samples (see Figure 1). Proximal samples were relatively easy to sample with bulk samples of the tephra being taken from the thick exposures. In addition, where present, accretionary lapilli were sampled from these thicker proximal to medial deposits in the hope that they had accreted a near-representative samples of the finer grained component of the bulk ash cloud material (Moore and Peck, 1962; Gilbert and Lane, 1994). For distal deposits, the often rather hard, cemented nature of the tephra made it possible to isolate small pods or biscuits of tephra (up to around 1-2 cm thick) which were shaved of any obvious adhering soil material with a knife to leave “clean” centimetre-sized pieces for analysis (see Figures 2E, 2F).

Figure 3 about here

Glass shards of the Lepué Tephra were separated from three cover-bed sequences, four lake cores and from ODP core 1233D, and prepared for analysis. Major elements were determined by EPMA at the Victoria University of Wellington, New Zealand, with 15 kV accelerating voltage, 8 nA beam current, and an electron beam defocused to between 20 to 10 µm. The same samples were subsequently analysed by laser ablation LA-ICP-MS at Aberystwyth University, Wales using a 20 µm

diameter crater from a 193 nm Excimer laser operating at 10 J cm^{-2} and 5 Hz, and calibrated using ^{29}Si as the internal standard against NIST SRM 612 and corrected for fractionation effects at the laser-sample interface (Pearce et al., 1997; Pearce et al., 2011; Pearce, 2014). Figure 3 illustrates the range of phenocryst content and vesicularity within the glass shards from the Lepué Tephra, dominated by plagioclase, with clinopyroxene and titanomagnetite. For many individual shards it is difficult to impossible to place a 10-20 μm diameter analysis (either by EPMA or LA-ICP-MS) on pure glass without encountering a phenocryst which will inevitably be included in the analysis. For both major and trace element analyses, the MPI-DING reference material ATHO-G (Jochum et al., 2006) was analysed as an unknown and gave both accurate and precise results (±5-10% for trace elements; between ±1-10% for major elements with the poorest analytical precision from the analyses of the minor elements Mn, Mg and Ti, present at 0.1-0.3 wt% oxide). Solution nebulisation (SN) ICP-MS trace element analyses were performed on a range of proximal and distal bulk cover-bed samples of Lepué Tephra including individual accretionary lapilli, and bulk samples from ODP core 1233D. Approximately 0.25 g of sample was digested in hot open $HF/HClO_4$, after grinding in an agate mortar and pestle, the solution made up to 250 mL in 2.5% HCl and analysed using an Agilent 7500 ICP-MS running in collision [He] mode. Analyses were performed alongside certified reference materials JA-3 (andesite) and QLO-1 (quartz latite) (see GeoReM, 2014), which gave results accurate to within ±2-5%. Full details of analytical methods are given by Alloway et al. (2017a), which should be consulted as the repository of compositional data used in this study. Major element data are presented in Alloway et al. (2017a), and trace element data are presented in the supplementary information to this paper, as well as Alloway et al. (2017a). X-ray diffraction (XRD) analyses were conducted on a selection of bulk samples covering the fall-out of the Lepué Tephra at the National Museum of Wales, Cardiff, using a Panalytical X'Pert XRD with peak recognition and mineral quantification achieved using Panalytical HighScore software, with a typical phase detection limit between 0.1% and 1%.

4. Mineralogy

Table 1 about here

The results from XRD analysis of the bulk samples indicate that the majority of phenocrysts in the Lepué Tephra are plagioclase (plag., and fitted by the Panalytical HighScore software as a disordered sodian anorthite composition - $[Ca_{0.83},Na_{0.17}](Si,Al)_4O_8$, from JCPDS File 00-041-1481), augite (aug.) and quartz (qtz, see Table 1). The average bulk mineralogical composition of accretionary lapilli and the bulk proximal Lepué Tephra samples (<40 km from Volcán Michinmahuida) are extremely similar

(accretionary lapilli - 32% aug., 61% plag., 6% qtz, 1% titanomagnetite (Ti-Mt); bulk tephra - 30% aug., 63% plag., 7% qtz). In the three distal tephra samples studied, there is a steady decrease in augite content and a concomitant increase in plagioclase with increasing distance from Volcán Michinmahuida. This mineralogical change coincides with a general thinning of the tephra and increasing alteration, with a colour change to more red-brown hues related to the oxidation of Fe. One accretionary lapillus has titanomagnetite recorded as a minor phase, and in the distal bulk tephra sample at 80 km from Volcán Michinmahuida, magnetite is recorded, most likely associated with weathering (hydration) of the tephra and oxidation of Fe^{2+}-bearing phases.

5. Compositional variation within the Lepué tephra

Alloway et al. (2017a) considered some aspects of the composition of the Lepué Tephra, using major element glass chemistry and a limited range of trace element data to show that this supported the stratigraphic (field-based) correlation of the various Lepué Tephra occurrences. However, it was apparent from this earlier study that the data were not straightforward, with problems (for both major and trace element single grain analyses) arising from the analysis of phenocrystic glass. The glass component of shards from all analysed samples is rhyolitic (~71 wt % SiO_2) when free of microphenocrysts, but when the shards contain numerous microlites, EPMA generates a basaltic-andesite "bulk shard" composition with ~55 wt % SiO_2 as a mix of rhyolitic glass and abundant phenocrysts (see Table 2 and Figures 18 and 19 in Alloway et al., 2017a). The pervasive alteration of the tephra during weathering and soil-forming processes alters the glass phase so that only a limited number of samples preserve material suitable for microbeam analysis, and has the potential to change the composition of the tephra by adding or removing mobile elements from the deposit. For these reasons Alloway et al. (2017a) in their tephra correlation study chose to provide only a limited discussion of the tephra bulk compositional data. In the present paper, the single grain trace element data (by LA-ICP-MS) are revisited, and compared with a fuller consideration of the bulk sample trace element data to provide a robust geochemical correlation based on trace elements which are both incompatible and immobile, and thus have inter-element ratios which (i) are immune from the effects produced by incorporation of phenocrysts in microbeam analyses and (ii) remain essentially unchanged during weathering. These elements form a subset of those high field strength elements (e.g. Y, Zr, Nb, REE, Hf, Ta, Th, U) that are generally regarded to be (but do not always behave as) both incompatible and immobile. The truly incompatible and immobile elements will be shown to provide a means to correlate phenocryst-rich, deeply weathered tephra deposits such as the Lepué Tephra that are challenging from an analytical perspective.

Figure 4 about here

5.1 Single grain trace element analyses

Figure 4 shows a selection of LA-ICP-MS trace element data from analyses of single shards of the Lepué Tephra. The Sr-Zr data (Figures 4A, 4B) range from ~ 100 ppm to 1150 ppm Sr which correlates with a steady decrease in Zr from around 650 ppm to ~25 ppm. This relationship relates to an increasing proportion of phenocryst material (largely plagioclase) and a reduction in the amount of glass ablated from the shard. Plagioclase feldspar has a high distribution coefficient (Kd) for Sr, which substitutes readily for Ca, with Kds in rhyolites and dacites ranging from 2.25-20, but has a low Kd in augite ~0.5 (GERM, 2013). In contrast, Zr is incompatible in both plagioclase (Kd ~0.15) and augite (Kd ~0.25). Incorporation of increasing amounts of a mixture of 2:1 plagioclase: augite in the ablated material (proportions taken from XRD mineral abundances) will cause Sr to increase and Zr to decrease compared to their concentrations in pure, microlite-free rhyolitic glass analyses (Pearce, 2014). The pure glass, which represents the frozen melt phase present at the time of eruption, forms the cluster of analyses at <113 ppm Sr and between ~570-770 ppm Zr (see Figures 4A, 4B). Figure 4C shows Zr-Y data. At the highest Zr concentrations (>~600 ppm Zr) analyses from all samples are coincident and are of the pure glass phase, whereas in samples contaminated by the presence of increasingly abundant phenocrysts (<~500 ppm Zr) the data spread out, with higher Y concentrations in the more distal samples from ODP core 1233D and Lago Lepué. Yttrium is compatible in augite in rhyolitic magmas (Kds 2.6-7.6, GERM, 2013) and this spread in Y concentrations is likely to be the result of the incorporation of higher quantities of augite in the ablated material. The difference from the more proximal samples from Lago Paso Blanco, Puente Aguila and La Zeta, Esquel, may reflect differences in the mineralogical composition of the magma (particularly the augite:plagioclase ratio) from different phases of the eruption, particularly from the later eruption of less compositionally evolved magma in a zoned magma body (see Alloway et al., 2017a). This behaviour is also shown by the REE, where the middle (M)REE (e.g. Gd, Ho, Er) show similar behaviour to Y and are more compatible in augite (Rollinson, 1993; GERM, 2013) than the light (L)REE (La, Ce) and heavy (H)REE (Yb, Lu) which compare better with the more proximal samples. Figures 4D and 4E show data for Zr-Th and Zr-Nb from single glass shards. Thorium and Nb, like Zr, are highly incompatible elements with very low Kds into plagioclase and augite, and because of this they show consistent ratios to Zr, giving a tightly clustered array of data spreading from low concentrations where the analysed shard contained abundant phenocrysts, to the pure glass (i.e. magmatic) composition at high Zr contents. The consistency of these ratios, and equally the ratios of other incompatible elements in the glass shards such as Hf, Ta, REE, and U, supports the correlation of all of these Lepué Tephra samples.

Figure 5 about here

The dilution effect of the incorporation of phenocrystic material is also seen in chondrite-normalised average REE data for all single shard analyses (Figure 5A). REE data from individual samples show similar, parallel patterns and slopes, but average concentrations vary by a factor of about 2 because of the dilution from phenocryst ablation. When only the low Sr (<113 ppm) analyses are averaged (Figure 5B), these represent the composition of the pure (phenocryst-free) glass phase (i.e. the quenched magma), which has a higher average REE concentration, and the separate samples show a narrower compositional range. No analyses of Lepué Tephra glass from Lago Lepué and only two analyses from ODP core 1233D have less than 113 ppm Sr, indicative of the high phenocryst contents in these later erupted, more distal deposits (Alloway et al., 2017a), presumably sourced from a deeper, less evolved portion of the magma body feeding the eruption. As well as higher overall REE, these low-Sr glass analyses also show a deeper negative Eu anomaly than the average of all data, a result of the preferential incorporation of Eu^{2+} into plagioclase (which is excluded from the low Sr averages). These data also confirm the regional correlation of the Lepué Tephra, but are limited to a few proximal sites and cores where fresh glass samples could be obtained: no fresh glass was recovered from the highly weathered, thin distal deposits from, for example, Isla Grande de Chiloé. To assess the correlation of these deposits, bulk analyses of proximal and distal deposits were performed.

5.2 Bulk sample and accretionary lapilli trace element analyses

Figure 6 shows a selection of trace elements plotted against Zr from solution nebulisation ICP-MS analyses of bulk tephra and individual accretionary lapilli from the Lepué Tephra, grouped according to depositional distance from Volcán Michinmahuida. Other weathered tephra layers which are stratigraphically associated with the Lepué Tephra, and from field evidence were interpreted to be of a Volcán Michinmahuida source (e.g. Figure 2C) are plotted for comparison: they are not correlatives of the Lepué Tephra, but nonetheless show similar compositional attributes (Alloway et al., 2017a). Rubidium vs Zr (Figure 6A) show a very wide spread of the data, with the distal samples showing low Rb at high Zr, although many of the proximal samples and accretionary lapilli are of similar composition. Rubidium is a soluble and mobile alkali metal, and in the highly altered and oxidised distal samples it is likely to have been removed in solution from the original tephra, while Zr (insoluble) will not have been affected, remaining in the tephra as an immobile element. It is thus possible that Zr may have been concentrated during the weathering of the tephra by the relative loss in mass through dissolution by hydrolysis of original glass and mineral components, taking soluble components such as the alkalis, Ca and Mg (as dissolved ions) and silica (as silicic acid) from the tephra during weathering (Faure, 1998; Churchman and Lowe, 2012). This oxidative weathering would leave a leached residue also relatively enriched in “insoluble” Al and Fe and Mn (Tardy and

Nahon, 1985). In contrast, two bulk samples of Lepué Tephra from ODP core 1233D (core depths of 14.68 m and 14.80 m, each analysed in triplicate) shows Rb concentrations about twice the average of proximal bulk and accretionary lapilli samples. The high Rb in the ODP 1233D core sample seems most likely to result from the mixing of marine clays, generally rich in Rb (Li and Schoonmaker, 2003) into the tephra layer by bioturbation and/or co-deposition (Todd et al., 2014). Because of this, the analysis of a bulk sample of this marine occurrence of distal tephra (a mixture of tephra and marine clay) is likely to not be fully representative of the deposit as a whole, but no samples of the enclosing marine sediment were analysed in this study, and no sediment composition data from ODP core 1233D have been published. The individual glass shard chemistry (from unaltered glass, which is frequently well-preserved in marine sediments) however clearly identifies it as Lepué Tephra (see above).

Figure 6 about here

Yttrium is plotted against Zr from bulk tephra analyses in Figure 6B and this, somewhat unexpectedly, shows a wide spread of the Y compositions. More commonly Y would generally be expected to show a good correlation with Zr showing a well-defined, consistent ratio (e.g. Pearce et al., 2002; Alloway et al., 2015; Alloway et al., 2017b; Martin-Jones et al., 2017b). This is a result of Y being generally both incompatible and immobile, although in some circumstances it can be incorporated in some phenocryst phases, e.g. augite (with MREE, see above) and amphibole or garnet at high pressure (e.g. Harangi et al., 2007), although these are not observed in the Lepué Tephra . Notably for the Lepué Tephra, the distal cover-bed deposits show the lowest Y/Zr ratios (i.e. lowest Y) whist the proximal samples and accretionary lapilli are similar in composition, and this behaviour is also seen with Rb (Figure 6A). This reduction in concentration of Y in distal deposits suggests that it too has been mobilised during alteration of the tephra in this hyper-humid high-weathering environment. Similar behaviour to Y is shown by all the REE, which also have the lowest concentrations in the distal deposits (see data in Alloway et al., 2017a). Uranium (Figure 6C) shows a moderate spread in concentrations and U/Zr ratio with the distal samples showing the lowest U/Zr ratio but the distal samples do not show the marked depletion displayed by Y and the REE.

However U, like Rb, in the ODP 1233D core samples is about twice the concentration of proximal and accretionary lapilli bulk analyses, and this is again consistent with mixing with marine sediments which are generally relatively high in U (Li and Schoonmaker, 2003). This is particularly true if the marine sediments are rich in organic material which promotes the reduction of the conservative uranyl tricarbonate species present in oxic sea water causing the precipitation of uraninite (Pattan and Pearce, 2009). OF the terrestrial deposits, the proximal Lepué Tephra samples have the highest U/Zr ratio, with lower U/Zr in distal samples and some accretionary lapilli, which is consistent with

oxidative weathering causing mobilisation of U. This is reflected in the general reddening of distal deposits which results from the formation of insoluble Fe-oxides (presumably hematite, ferrihydrite, or maghemite, e.g. Churchman and Lowe, 2012). Thorium and Nb are plotted against Zr in Figures 6D and 6E, and show highly consistent ratios to Zr across the fall-out range, with no discernible difference between proximal, distal or accretionary lapilli samples, apart from the higher Th in the ODP 1233D samples, which can again be attributed to mixing with marine sediment where Th is generally associated with the detrital clay fraction (Myers and Wignall, 1987). It is notable that both Nb and Th are highest in the weathered, distal occurrences of the Lepué Tephra, again suggesting their relative enrichment in insoluble phases (behaviour similar to Zr), resulting from the removal by leaching of the more soluble components of the deposit, these "mobile" elements here including REE, Y and U.

Figure 7 about here

The REE data from the bulk Lepué Tephra analyses are presented in Figure 7, averaged as groups according to their occurrence or depositional distance from Volcán Michinmahuida. There is a clear variation in the overall REE content of the samples with the highest concentrations shown by the accretionary lapilli and the proximal samples, with low concentrations in ODP core sample 1233D and in the distal samples. Modest negative Eu-anomalies are displayed in all samples, a result of the extraction of feldspar during the evolution of the parent magma, and a distinct positive Ce-anomaly is shown by the distal samples. The low concentrations in the ODP 1233D core sample may relate to dilution of the primary tephra by marine sediment. In the distal samples, low REE concentrations are related to mobility in these particular weathering conditions (*cf*. mobility of Y described above). In contrast to the LA-ICP-MS glass data, the bulk sample REE data (Figure 7) do not show smooth normalised curves (*cf.* Figure 5), but are more irregular displaying a series of evenly spaced "humps" and intervening "cusps" with increasing atomic number. These features are most notable in the proximal and distal terrestrial (cover-bed) samples and in the accretionary lapilli, with the cusps between Nd-Pm, at Gd, and between Ho-Er, but these are not displayed by the ODP 1233D core samples. This is a manifestation in the REE of the "tetrad effect" (Peppard, 1969; Bau, 1996) where deviations from a smooth, steady change in REE behaviour related to ionic radius contraction occurs to give cusped REE chondrite-normalised patterns. This behaviour, often referred to as non-CHARAC – i.e. non-*CHA*rge-*RA*dius *C*ontrolled (Bau, 1996) – results from the increased stability of REE ions at quarter, half, three-quarter, and complete filling of the 4f electron shell and these effects have been observed in a range of natural samples. Examples of the occurrence of tetrad effects in the REE which may be relevant to the study of the weathered Lepué Tephra encompass magmatic processes in granite magmas including late stage fractional crystallisation (Irber, 1999; Zhenhua et al., 2002);

extended groundwater interaction and alteration of granitic rocks (Masuda and Akagi, 1989; Takahashi et al., 2002); co-precipitation of REE in Fe-Mn oxyhydroxides from solution (Bau, 1999; Kawabe et al., 1999); processes occurring during argillic alteration (Abedini et al., 2018a) and the formation of Ti-rich bauxites (Abedini et al., 2018b), and during chemical weathering associated with the formation of *terre rosse* (Feng, 2010; Feng et al., 2011).

In the case of the Lepué Tephra, the formation of a tetrad effect during any late-stage magmatic processes can be excluded as the individual glass shard chemistry shows no signs of any tetrad or non-CHARAC effects (see Figure 5B). The Lepué Tephra displays "M-type" tetrad effects, where the cusps form low points between convex-upward curved segments and this pattern has been described in weathered materials with the opposite "W-type" curve being reported in groundwater (Masuda and Ikeuchi, 1979; Masuda et al., 1987; Takahashi et al., 2002). The evidence indicates that post-depositional terrestrial weathering in the soil-forming environment generated the observed REE distributions within the Lepué Tephra. This finding is further supported by consideration of REE behaviour in Fe-oxyhydroxides that formed in the altered Lepué Tephra to generate the red-orange brown colouration. Secondary Fe-Mn oxyhydroxides formed during weathering or alteration frequently display strongly developed tetrad effects (Bau, 1999; Kawabe et al., 1999; Feng, 2010; Feng et al., 2011; Abedini et al., 2018b). In addition Fe-Mn oxyhydroxides, formed by precipitation from oxidising waters, will also preferentially concentrate Ce^{4+}, the oxidised form of Ce, which can lead to the generation of a positive Ce anomaly (Bau, 1999; Leybourne and Johannesson, 2008; Bau and Koschinsky, 2009; Feng, 2010) as is observed in the distal cover-bed Lepué Tephra deposits (see Figure 7). The bulk sample REE data from ODP core 1233D shows neither any tetrad effect nor any significant Ce anomaly, and again this indicates that these features in the cover-bed samples are not primary magmatic features, but must be associated with surface, post-depositional processes which do not affect the marine-deposited ODP core sample.

Figure 8 about here

Figure 8 shows the magnitude of any Ce anomaly (expressed as Ce/Ce*) present in both the glass analyses by LA-ICP-MS and the bulk sample analyses by SN-ICP-MS grouped by depositional distance from Volcán Michinmahuida plotted against La (in ppm) from the Lepué Tephra. The Ce anomaly is calculated here by $Ce/Ce^* = 2\log Ce_N / (\log La_N + \log Pr_N)$ where Ce_N etc. represents the chondrite normalised concentration. Ce/Ce* >1 indicates a positive Ce anomaly. The single glass shard analyses show little or no Ce anomaly, clustering around Ce/Ce* ~1, with La decreasing from about 60 ppm in the pure glass phase (i.e. the magmatic composition) to a few ppm as increasing amounts of phenocryst are incorporated in the analyses (La, and other REE are moderately to highly incompatible in the major phenocryst phases in the Lepué Tephra). In the bulk analyses of cover-bed

samples, however, it is clear that the magnitude of the Ce anomaly increases as the La concentration decreases, with the majority of distally-deposited samples showing a marked positive Ce anomaly (Ce/Ce* up to ~1.5) and low La. This results from the leaching of trivalent REE (including La and Pr) from the samples while Ce (present as Ce^{4+} in this oxidising weathering environment) is retained, most likely to be sorbed on to an Fe-oxyhydroxide phase (Bau, 1999; Feng, 2010). Even some of the thicker, proximal cover-bed deposits, and some accretionary lapilli show a reduction in La (and other LREE) compared to a typical bulk composition of around 30 ppm, the reduced Le and Pr generating an increase in Ce/Ce*, indicating that some of these samples also did not escape the ravages of this oxidative chemical weathering.

6. Chemical correlation of the Lepué Tephra

With only a limited number of samples from which fresh glass could be recovered for single grain analyses, and the problems of extensive weathering noted in bulk sample analyses where mobility of elements generally regarded as immobile such as the REE can be observed, it is appropriate to ask whether geochemistry can be used to correlate the Lepué Tephra across its entire fallout region. The direct comparison of single-grain and bulk sample trace element analyses have been widely cautioned against because of the problems of variable amounts of phenocryst incorporation in LA-ICP-MS analyses, and the possibility for incorporation of non-juvenile material, alteration and/or various sedimentary fractionation effects in bulk tephra analysis can complicate their interpretation (Pearce et al., 2002; Pearce et al., 2007; Pearce et al., 2008; Pearce, 2014; Pearce et al., 2014; Martin-Jones et al., 2017a). The Lepué Tephra provides an excellent opportunity to test the use of such data sets in correlation studies.

Figure 9 about here

Figure 9 compares selected bulk and single grain glass shard trace element data from all samples of the Lepué Tephra determined by either SN-ICP-MS or LA-ICP-MS. The concentrations of the elements determined from the bulk samples are both lower and more limited in range than the glass shard data, because the bulk samples are a mix of glass and mineral (maybe with or without lithics) material whereas the single shard data records the range from the pure glass to almost entirely mineral compositions (where microphenocrysts are abundant). However, for the highly incompatible and immobile elements (Zr, Nb, Th, Hf, and Ta, Figures 9A-9C) inter-element ratios are identical for the bulk samples and single shard analyses. For example, Zr/Th is 48.3 ± 8.7 in the bulk sample analyses, and 47.1 ± 6.5 in the single shards, and Zr/Nb is 22.8 ± 4.5 in the bulk sample analyses, and 23.6 ± 3.2 in the single shards. These ratios therefore allow the comparison of bulk analyses with

single grain data, and confirm the correlation of the Lepué Tephra across its fall-out despite using a mix of data from different analytical methods. Although the Ta data shows a wider spread in LA-ICP-MS data because of the lower instrument sensitivity (Pearce et al., 2004), the ratio Hf/Ta is also indistinguishable between the two sets of data (i.e. bulk and single-grain analyses). In contrast, Figures 9D-9F show the comparison for the two analytical methods for least one element per graph which is mobile in the soil-forming environment (e.g. Sr, La, Rb, Cs), and it is clear that the single-grain data cannot be compared with the bulk analyses for these mobile elements. Thus, while limited confirmation of the correlation of the Lepué Tephra was achieved using a few samples by Alloway et al. (2017a), confirming the stratigraphic, field and morphological correlations, the comparison here of element pairs from Zr, Hf, Nb, Ta, and U to give ratios, which are neither influenced by the presence of phenocrysts in the ablated material, nor by weathering in the cover-bed succession, provides a more robust method of correlation using this multi-method analytical approach.

Incompatible trace element ratios from the Lepué Tephra also differ from other Holocene tephra deposits in the same region. The slightly younger Chana Tephra, *ca* 9750 cal a BP (Alloway et al., 2017b), previously widely referred to as Cha-1, closely overlies the Lepué Tephra at many sites and has Zr/Nb of 8.4 ± 9 and Zr/Th of 5.6 ± 0.4 (162 LA-ICP-MS individual glass shard analyses), both much lower and distinct from the Lepué Tephra. Pumices from an early Holocene (~11.7 ka cal BP) tephra deposit (RMV) erupted from the Volcán Mentolat, southern Chile, have Zr/Nb of 24.9 ± 3.7 and Zr/Th of29.7 ± 3.7 (Weller et al., 2019), again different from the Lepué Tephra. Three younger (late Holocene) tephra deposits from Volcán Melimoyu have bulk sample (solution ICP-MS analyses) Zr/Nb ratios of 18.2 ± 0.1 (Mm-1p), 18.1 ± 0.1 (Mm-1s) and 18.7 ± 0.6 (Mm-2), and Zr/Th ratios of 38.3 ± 0.2 (Mm-1p), 45.5 ± 0.5 (Mm-1s) and 34.8 ± 2.1 (Mm-2) (Geoffroy et al., 2018), and again the ratios differ significantly from the Lepué Tephra. Thus, these highly incompatible element ratios may also serve to identify individual sources in the area, and allow discrimination between tephra deposits. As yet, there are no data from the closely associated intensely weathered scoriaceous lapilli tephra deposits from other local volcanoes which are likely to include Volcánes Corcovado, Yate or Calbuco (see Figure 2C).

7. Conclusions

The elements Zr, Nb, Hf, Ta, and Th are highly incompatible in igneous systems, preferring to remain in the magma rather than entering crystallising phases, even in relatively evolved rhyolitic magmas, prior to the onset of zircon or other accessory phase crystallisation. This is the case for the ~71% SiO_2

magma (containing abundant phenocrysts to give an overall intermediate bulk-rock composition), which erupted to form the Lepué Tephra. Many other elements also behave incompatibly in rhyolitic magmas (for example, the REE, Y, and U), but of the incompatible elements it is only Zr, Nb, Hf, Ta, and Th, which remain immobile once exposed to weathering after deposition in the hyper-humid andic soil-forming environment prevalent in this region of northern Patagonia/southern Chile. In these hyper-humid, oxidising conditions the REE, Y and U become mobilised, with significant fractionation of the REE occurring to leave weathered cover-bed tephra deposits with irregular chondrite normalised REE patterns and positive Ce anomalies. These features result from the non-CHARAC behaviour of the REE and the preferential sorption of Ce^{4+} onto secondary Fe-oxyhydroxides precipitated as residual phases during the alteration of the tephra. The effects of this sub-aerial oxidative weathering are most extensive on the thinner, more distal terrestrial tephra deposits, but even some of the thicker, proximal deposits (which may be up to ~2 m thick) are not immune to the compositional changes imparted by weathering, as observed in some of the accretionary lapilli bulk sample analyses. The ODP 1233D core sample is, however, unaffected by weathering, but its bulk composition would appear to include incorporated marine sediment relatively rich in U, Th and Rb, which moves if away from the bulk analyses of the Lepué Tephra. However, data from unaltered glass shards within the tephra samples from ODP 1233D indicates this is clearly Lepué Tephra.

For the terrestrial deposits of the Lepué Tephra, only a few cover-bed samples yield glass shards suitable for LA-ICP-MS trace element analysis, and intense weathering by hydrolysis and high rainfall have resulted in the leaching of elements (solutes) from the bulk tephra making straightforward comparisons of bulk analyses problematic. Because of this alteration and loss by leaching, chemical correlation across the entirety of the tephra fall cannot easily be achieved by consideration of data from only one analytical method. The consideration of a set of ratios for elements that are both incompatible and immobile, however, allows data from bulk and single grain analytical methods to be compared. For the fall-out region of the Lepué Tephra, it is the ratios of Zr, Nb, Hf, Ta, and Th that provide a basis for robust correlation and inter-method comparison, particularly when chemical correlations are considered alongside detailed stratigraphic information. These elements are only a subset of those elements generally considered to be immobile, a group which would typically also include the REE, Y, and U. In considering the compositional data from the Lepué Tephra, Alloway et al. (2017a) concluded that “These results indicate the limited utility of bulk analyses in the absence of associated chronostratigraphic contexts to be able to adequately differentiate [Volcán Michinmahuida]-sourced eruptives”. While there are certainly challenges in interpreting bulk chemical data, particularly from such variably altered, intermediate tephra deposits, the careful consideration of the data (as presented here) can allow reliable correlations to be made, which

substantiate the stratigraphic information, and can allow these bulk analyses to be linked in to the single-grain glass shard chemistry. Consideration of Zr, Hf, Nb, Ta and Th in this high weathering environment specifically overcomes the issue of element mobility (as displayed by the REE here), and their incompatibility allows for robust inter-method comparisons. In the case of the Lepué Tephra, the behaviour of the more mobile elements in this setting (e.g. the REE) from bulk sample analysis also gives an indication of the conditions (i.e. oxidising) in which the weathering occurred. Thus, in the most unpromising of analytical or geochemical conditions, ratios of the highly incompatible and immobile elements (Zr, Hf, Nb, Ta, Th) enable the comparison of bulk and single grain analyses, and provide a means for robust compositional tephra correlation, while the REE, Y, U are mobilised by weathering in these hyper-humid soil-forming environments and must be regarded accordingly. This approach using element ratio data from bulk and single grain analyses for immobile incompatible elements has great potential in the study of weathered, phenocrystic tephra deposits. This new approach is especially important in helping enable such variably weathered tephras to be correlated over much great distances than previously attained, and hence their usefulness as chronostratigraphic tools in multiple Quaternary-related studies is considerably enhanced.

Acknowledgements

This study was funded in part by grants from Aberystwyth University Research Fund to NJGP and a Victoria University of Wellington Science Faculty Research Grant to BVA. Some fieldwork undertaken by BVA was also funded by Iniciativa Cientifica Milenio grants P02-51 and NC120066, Fondecyt 1151469 to Patricio Moreno, Universidad de Chile, Santiago. Richard Bevins and Tom Cotterell at the National Museum of Wales, Cardiff, are thanked for assisting NJGP with the XRD analyses and providing facilities during a period of research leave. At Aberystwyth University, Andy Brown at DGES, is thanked for assisting with/conducting solution-ICP-MS analyses and Ron Fuge is thanked for his comments on an earlier draft of this manuscript. We would like to thank the two QI referees (David Lowe, University and Waikato and anonymous) for their comments, and also Andrei Sarna-Wojcicki, USGS, for his additional and insightful comments, all of which have helped clarify and improve this contribution.

530 **Tables**

531

532 **Table 1.** Mineralogical abundances (%) in samples of Lepué Tephra measured by X-ray diffraction.
533 "Na-An" is a plagioclase of sodian anorthite composition from JCPDS Data File 00-041-1481.
534 Distances measured as straight line from the top of Volcán Michinmahuida. Abbreviations: Qtz-
535 quartz; Ti-Mt – titanomagnetite; Mt – magnetite. Other phases identified as present in the Lepué
536 Tephra are listed, but these are <~1%, and in some cases these more exotic mineral species are likely
537 to be an artefact of the software peak fitting at such low abundances. Nanocrystalline minerals,
538 namely allophane and ferrihydrite, together with hydrous Fe-oxides (e.g. haematite) are likely to be
539 present in these andic soils (Churchman and Lowe, 2012), but will not be specifically identified by
540 XRD in this study.

541

Sample	Dist. km	Aug.	Na-An	Qtz	Ti-Mt	Mt	Other phases reported at trace amounts (treat identification with caution)
Proximal							
Pum 4-1	18	22	71	7			Tremolite, leifite
S5.1	22.5	37	56	6			
15J13S9C	31	29	65	6			
11J13S12-T2	38	33	60	8			Broad clay "peak" at 10° 2θ
Distal							
9J13S5-T1	80	35	57	6		3	
8J13S2-T1	120	23	73	4			Leifite, eckermannite, rouvillite (carbonate)
Chapo Rd S1-1	144	0	94	6			Humite, pigeonite?
Accretionary lapilli (proximal)							
S8.3 (5)	25	25	68	7			Nimesite (clay kaolinite-serpentinite group)
S9.1 (13)	29	30	64	1	4		
S13.1 (1)	38.5	31	59	10			
Cor-1 S1 (2)	41	41	53	6			Lizardite (clay kaolinite-serpentinite group)

542

Figures – submitted as 2400 dpi eps files

Figure 1. Map of the study area indicating the distribution and sample locations of the Lepué Tephra. Open red circles are lake cores occurrences, open green diamonds are thin (typically <10 cm) tephra samples from cover-bed sequences referred to as "distal" from Volcán Michinmahuida, and open blue squares are thicker tephra samples (>> 30 cm) from cover-bed sequences "proximal" to Volcán Michinmahuida. ODP sites 1233D is marked where a 12 cm thick layer of Lepué Tephra is recorded. Dashed ellipse marks the 1 cm isopach, and is the approximate extent of Lepué Tephra in visible in cover-bed sequences. Thickness data for individual occurrences, locality information and stratigraphic logs can be obtained from Alloway et al. (2017a). Abbreviations: ***L. Ll.*** – Lago Llanquihue, ***V. Mm.*** – Volcán Melimoyu (see Geoffroy et al., 2018), ***V. Ch.*** – Volcán Chaiten (see Alloway et al., 2017b), ***V. Co.*** – Volcán Corcovado.

Figure 2. The range of field occurrences of Lepué Tephra throughout northwest Patagonia. For locality and stratigraphic information pertaining to each site see Alloway et al. (2017a). **A.** Proximal occurrence just north of Chaitén (Section 8, 17 km west of Volcán Michinmahuida). Lower arrow indicates the weathered scoriaceous orange lapilli-rich basal layer (magmatic phase) of Lepué Tephra eruption, whereas the upper arrow indicates the grey poorly sorted massive to weakly stratified scoriaceous ash layer (phreatomagmatic phase). **B.** Accretionary lapilli in proximal deposit from Section 8, the largest here are ~2.5 cm in diameter. **C.** Massive grey Lepué Tephra (arrowed) (Section 1, 40 km south of Volcán Michinmahuida) enveloped by strongly weathered orange-coloured pumice-lapilli rich tephra beds and andic soil interbeds. Spade (marked) for scale (~ 1m long) resting on lower bedrock exposure. **D.** Distal Lepué Tephra, 12 cm thick, from La Paloma, 170 km NNW of Volcán Michinmahuida, just north of Puerto Montt. **E.** Lepué Tephra forming discontinuous cemented ash pods overlying glacial deposits at Queilen, Isla Grande de Chiloé , 85 km west of Volcán Michinmahuida. **F.** Lepué Tephra forming subtle discontinuous cemented ash pods ~ 3 cm in diameter (inclined arrows), approximately 30 cm below the diffuse white rhyolitic distal 9.7 ka Chana Tephra (between upper horizontal arrows, formerly Cha-1, see Alloway et al., 2017b) at the Cholgo section, 85 km north of Volcán Michinmahuida. This is Section A of Watt et al. (2011), but they do not record the occurrence of any tephra below the Chana Tephra. Knife is 20 cm long.

Figure 3. Back scattered electron images of individual glass shards from the Lepué Tephra, showing the range of microlite contents and vesicularity in pairs of shards from three samples: **A-B** – Lago Lepué, Chiloé (distal); **C-D** – ODP core 1233D (distal); **D-E** – Puente Aguila Road Section 5, ~20 km NNW of Volcán Michinmahuida (proximal) (see Figure 1 and Alloway et al., 2017a). In each case low microlite contents are illustrated on the upper row (**A, C, E**) and high microlite contents on the lower row (**B, D, F**). Note different scale bars for different images of either 10 µm (**A, C, D**) or 100 µm (**B, E, F**). In microlite rich samples (and some samples with relatively "low" microlite contents), it is impossible to place a 20 µm diameter LA-ICP-MS analysis without ablating phenocrystic material.

Figure 4. Plots of selected trace element concentrations for single glass shard analyses determined by LA-ICP-MS. See text for discussion. All concentrations in ppm.

Figure 5. A. Plot of chondrite-normalised average composition of REE for all single shard analyses of samples analysed by LA-ICP-MS. **B.** Plot of chondrite-normalised average composition of REE for samples analysed by LA-ICP-MS with <113 ppm Sr, i.e. those analyses of "pure" glass, free from the ablation of phenocrystic material. Note no samples from Lago Lepué have less than 113 ppm Sr. See text for discussion. Chondrite compositions from Sun and McDonough (1989).

Figure 6. Plots of selected trace elements against Zr for solution nebulisation ICP-MS analyses of bulk tephra and individual accretionary lapilli from the Lepué Tephra. Analyses are grouped according to depositional distance from Volcán Michinmahuida (see Figure 1). "Associated tephra" indicates other weathered tephra layers stratigraphically associated with the Lepué Tephra (see for example Figure 2C) and, based on field evidence, were initially interpreted to be of a Volcán Michinmahuida source (Alloway et al., 2017a). All concentrations in ppm.

Figure 7. Chondrite-normalised average composition of REE for grouped Lepué Tephra deposits, analysed by SN-ICP-MS. Some groups show the presence of "M-type" tetrad effects, notably between Gd and Lu in proximal, distal and accretionary lapilli samples (note the relatively high concentrations of Tb and Tm-Yb compared to neighbouring REE). Arrows mark the boundaries between the four individual tetrads which include La-Nd, Sm-Gd, Gd-Ho and Er-Lu. The second tetrad (Sm-Eu) is often unclear as it includes Eu, which shows variable oxidation states leading to the common occurrence of anomalous behaviour in magmatic systems, and should include Pm, the highly radioactive REE which is no longer present at the Earth's surface. See text for discussion. Chondrite compositions from Sun and McDonough (1989).

Figure 8. The magnitude of any Ce anomaly (expressed as Ce/Ce* where values >1 indicate a positive Ce anomaly) compared to La concentration (in ppm) form the Lepué Tephra from both LA-ICP-MS analyses of single glass shards, and bulk analysis of samples by SN-ICP-MS, grouped by depositional distance/setting from Volcán Michinmahuida.

Figure 9. Comparison of selected trace element data from the Lepué Tephra determined by either LA-ICP-MS or SN-ICP-MS. For the highly incompatible and highly immobile elements (Zr, Nb, Hf, Ta, Th) element ratios are identical for the two methods applied and provide a means for correlation. All concentrations in ppm.

611 **References**

612 Abbott, P.M., Austin, W.E.N., Davies, S.M., Pearce, N.J.G., Hibbert, F.D., 2013.
613 Cryptotephrochronology of a North East Atlantic marine sequence over Termination II, the
614 Eemian and the last interglacial-glacial transition. Journal of Quaternary Science, 28: 501-
615 514.
616 Abedini, A., Azizi, M.R., Calagari, A.A., 2018a. The Lanthanide Tetrad Effect in Argillic Alteration: An
617 Example from the Jizvan District, Northern Iran. Acta Geologica Sinica, 92: 1468-1485.
618 Abedini, A., Calagari, A.A., Azizi, M.R., 2018b. The tetrad-effect in rare earth elements distribution
619 patterns of titanium-rich bauxites: Evidence from the Kanigorgeh deposit, NW Iran. Journal
620 of Geochemical Exploration, 186: 129-142.
621 Alloway, B., Neall, V., Vucetich, C., 1995. Late Quaternary (post 28,000 year BP) tephrostratigraphy
622 of northeast and central Taranaki, New Zealand. Journal of the Royal Society of New
623 Zealand, 25(4): 385-458.
624 Alloway, B.V., Moreno, P.I., Pearce, N.J.G., De Pol-Holz, R., Henriquez, W.I., Pesce, O.H., Sagredo, E.,
625 Villarosa, G., Outes, V., 2017a. Stratigraphy, age and correlation of Lepué Tephra: a
626 widespread *c*. 11,000 cal. A BP marker horizon sourced from the Chaitén Sector of southern
627 Chile. Journal of Quaternary Science, 36: 795-829.
628 Alloway, B.V., Pearce, N.J.G., Moreno, P.I., Villarosa, G., Jara, I., De Pol-Holz, R., Outes, V., 2017b. An
629 18,000 year-long eruptive record from Volcán Chaitén, northwestern Patagonia:
630 Paleoenvironmental and hazard-assessment implications. Quaternary Science Reviews, 168:
631 151-181.
632 Alloway, B.V., Pearce, N.J.G., Villarosa, G., Outes, V., Moreno, P.I., 2015. Multiple melt bodies fed the
633 AD 2011 eruption of Puyehue-Cordón Caulle, Chile. Scientific Reports, 5.
634 Bau, M., 1996. Controls on the fractionation of isovalent trace elements in magmatic and aqueous
635 systems: evidence from Y/Ho, Zr/Hf, and lanthanide tetrad effect. Contributions to
636 Mineralogy and Petrology, 123(3): 323-333.
637 Bau, M., 1999. Scavenging of dissolved yttrium and rare earths by precipitating iron oxyhydroxide:
638 experimental evidence for Ce oxidation, Y-Ho fractionation, and lanthanide tetrad effect.
639 Geochimica et Cosmochimica Acta, 63(1): 67-77.
640 Bau, M., Koschinsky, A., 2009. Oxidative scavenging of cerium on hydrous Fe oxide: evidence from
641 the distribution of rare earth elements and yttrium between Fe oxides and Mn oxides in
642 hydrogenetic ferromanganese crusts. Geochemical Journal, 43(1): 37-47.
643 Cas, R.A.F., Wright, J.V., 1987. Volcanic successions. Chapman and Hall, London, 528 pp.
644 Churchman, G.J., Lowe, D.J., 2012. Alteration, formation, and occurrence of minerals in soils. In:
645 Huang, P.M., Li, Y., Sumner, M.E. (Eds.), Handbook of Soil Sciences. 2nd edition. Vol. 1:
646 Properties and Processes. CRC Press (Taylor and Francis), Boca Raton, FL, pp. 20.1-20.72.
647 Cronin, S.J., Neall, V.E., Stewart, R.B., Palmer, A.S., 1996. A multiple-parameter approach to andesitic
648 tephra correlation, Ruapehu volcano, New Zealand. Journal of Volcanology and Geothermal
649 Research, 72(3-4): 199-215.
650 Donoghue, S.L., Vallance, J., Smith, I.E., Stewart, R.B., 2007. Using geochemistry as a tool for
651 correlating proximal andesitic tephra: case studies from Mt Rainier (USA) and Mt Ruapehu
652 (New Zealand). Journal of Quaternary Science: Published for the Quaternary Research
653 Association, 22(4): 395-410.
654 Faure, G., 1998. Principles and applications of geochemistry: a comprehensive textbook for geology
655 students. Prentice Hall, New Jersey, 600 pp.
656 Feng, J.-L., 2010. Behaviour of rare earth elements and yttrium in ferromanganese concretions,
657 gibbsite spots, and the surrounding terra rossa over dolomite during chemical weathering.
658 Chemical Geology, 271(3-4): 112-132.
659 Feng, J.-L., Gao, S.-P., Zhang, J.-F., 2011. Lanthanide tetrad effect in ferromanganese concretions and
660 terra rossa overlying dolomite during weathering. Chemie der Erde-Geochemistry, 71: 349-
661 362.

Geoffroy, C., Alloway, B.V., Amigo, À., Parada, M., Gutierrez, F., Castruccio, A., Pearce, N.J., Morgado, E., Moreno, P., 2018. A widespread compositionally bimodal tephra sourced from Volcán Melimoyu (44° S, Northern Patagonian Andes): Insights into magmatic reservoir processes and opportunities for regional correlation. Quaternary Science Reviews, 200: 141-159.

GeoReM, 2014. http://georem.mpch-mainz.gwdg.de/sample_query.asp.

GERM, 2013. Geochemical Earth Reference Model (GERM) Partition Coefficient (Kd) Database, www.earthref.org/KDD/.

Gilbert, J.S., Lane, S., 1994. The origin of accretionary lapilli. Bulletin of Volcanology, 56(5): 398-411.

Harangi, S., Downes, H., Thirlwall, M., Gméling, K., 2007. Geochemistry, petrogenesis and geodynamic relationships of Miocene calc-alkaline volcanic rocks in the Western Carpathian arc, eastern central Europe. Journal of Petrology, 48(12): 2261-2287.

Irber, W., 1999. The lanthanide tetrad effect and its correlation with K/Rb, Eu/Eu∗, Sr/Eu, Y/Ho, and Zr/Hf of evolving peraluminous granite suites. Geochimica et Cosmochimica Acta, 63(3-4): 489-508.

Jochum, K.P., Stoll, B., Herwig, K., others, 2006. MPI-DING reference glasses for in situ microanalysis: New reference values for element concentrations and isotope ratios. Geochemistry, Geophysics, Geosystems, 7: Q02008, doi:10.1029/2005GC001060.

Juvigné, É., Porter, S.C., 1985. Mineralogical variations within two widespread Holocene tephra layers from Cascade Range Volcanoes, USA. Géographie physique et Quaternaire, 39(1): 7-12.

Kawabe, I., Ohta, A., Ishii, S., Tokumura, M., Miyauchi, K., 1999. REE partitioning between Fe-Mn oxyhydroxide precipitates and weakly acid NaCl solutions: Convex tetrad effect and fractionation of Y and Sc from heavy lanthanides. Geochemical Journal, 33(3): 167-179.

Kirkman, J., McHardy, W., 1980. A comparative study of the morphology, chemical composition and weathering of rhyolitic and andesitic glass. Clay minerals, 15(2): 165-173.

Leybourne, M.I., Johannesson, K.H., 2008. Rare earth elements (REE) and yttrium in stream waters, stream sediments, and Fe–Mn oxyhydroxides: fractionation, speciation, and controls over REE+ Y patterns in the surface environment. Geochimica et Cosmochimica Acta, 72(24): 5962-5983.

Li, Y., Schoonmaker, J., 2003. Chemical composition and mineralogy of marine sediments, Treatise of Geochemistry. ElSevier, pp. 1-35.

Lowe, D.J., 2011. Tephrochronology and its application: a review. Quaternary Geochronology, 6: 107-153.

Lowe, D.J., Pearce, N.J.G., Jorgensen, M.A., Kuehn, S.C., Tryon, C.A., Hayward, C., 2017. Correlating tephras and cryptotephras using glass compositional analyses and numerical and statistical methods: review and evaluation Quaternary Science Reviews, 175: 1-44.

Lowe, D.J., Shane, P.A., Alloway, B.V., Newnham, R.M., 2008. Fingerprints and age models for widespread New Zealand tephra marker beds erupted since 30,000 years ago: a framework for NZ-INTIMATE. Quaternary Science Reviews, 27(1-2): 95-126.

Martin-Jones, C.M., Lane, C.S., Pearce, N.J.G., Smith, V.C., Lamb, H.F., 2017a. Recurrent explosive eruptions from a high-risk Main Ethiopian Rift volcano throughout the Holocene. Geology.

Martin-Jones, C.M., Lane, C.S., Pearce, N.J.G., Smith, V.C., Lamb, H.F., Oppenheimer, C., Asrat, A., Schaebitz, F., 2017b. Glass compositions and tempo of post-17 ka eruptions from the Afar Triangle recorded in sediments from Lake Ashenge and Lake Hayk, Ethiopia. Quaternary Geochronology, 37: 15-31.

Masuda, A., Akagi, T., 1989. Lanthanide tetrad effect observed in leucogranites from China. Geochemical Journal, 23(5): 245-253.

Masuda, A., Ikeuchi, Y., 1979. Lanthanide tetrad effect observed in marine environment. Geochemical Journal, 13(1): 19-22.

Masuda, A., Kawakami, O., Dohmoto, Y., Takenaka, T., 1987. Lanthanide tetrad effects in nature: two mutually opposite types, W and M. Geochemical Journal, 21(3): 119-124.

McHenry, L.J., Mollel, G.F., Swisher III, C.C., 2008. Compositional and textural correlations between Olduvai Gorge Bed I tephra and volcanic sources in the Ngorongoro Volcanic Highlands, Tanzania. Quaternary International, 178(1): 306-319.

Moore, J.G., Peck, D.L., 1962. Accretionary lapilli in volcanic rocks of the western continental United States. The Journal of Geology, 70(2): 182-193.

Myers, K.J., Wignall, P.B., 1987. Understanding Jurassic organic-rich mudrocks—new concepts using gamma-ray spectrometry and palaeoecology: examples from the Kimmeridge Clay of Dorset and the Jet Rock of Yorkshire, Marine clastic sedimentology. Springer, pp. 172-189.

Naranjo, J.A., Stern, C.R., 2004. Holocene tephrochronology of the southernmost part (42 30'-45 S) of the Andean Southern Volcanic Zone. Revista geológica de Chile, 31(2): 224-240.

Parfitt, R., Russell, M., Orbell, G., 1983. Weathering sequence of soils from volcanic ash involving allophane and halloysite, New Zealand. Geoderma, 29(1): 41-57.

Pattan, J.N., Pearce, N.J.G., 2009. Bottom water oxygenation history in southeastern Arabian Sea during the past 140 ka: Results from redox-sensitive elements. Palaeogeography, Palaeoclimatology, Palaeoecology, 280: 396-405.

Pearce, N.J.G., 2014. Towards a protocol for the trace element analyses of glass from rhyolitic shards in tephra deposits by laser ablation ICP-MS. Journal of Quaternary Science, 29: 627-640.

Pearce, N.J.G., Abbott, P.M., Martin-Jones, C., 2014. Microbeam methods for the analysis of glass in fine grained tephra deposits: a SMART perspective on current and future trends. In: Austin, W.E.N., Abbott, P.M., Davies, S.M., Pearce, N.J.G., Wastegard, S. (Eds.), Marine Tephrochronology. Geological Society Special Publication, London.

Pearce, N.J.G., Bendall, C.A., Westgate, J.A., 2008. Comment on "Some numerical considerations in the geochemical analysis of distal microtephra" by A.M. Pollard, S.P.E. Blockley and C.S. Lane. . Applied Geochemistry, 23: 1353-1364.

Pearce, N.J.G., Denton, J.S., Perkins, W.T., Westgate, J.A., Alloway, B.V., 2007. Correlation and characterisation of individual glass shards from tephra deposits using trace element laser ablation ICP-MS analyses: current status and future potential. Journal of Quaternary Science, 22: 721-236.

Pearce, N.J.G., Eastwood, W.J., Westgate, J.A., Perkins, W.T., 2002. The composition of juvenile volcanic glass from the c. 3,600 B.P. Minoan eruption of Santorini (Thera). Journal of the Geological Society, 159: 545-556.

Pearce, N.J.G., Perkins, W.T., Westgate, J.A., Gorton, M.P., Jackson, S.E., Neal, C.R., Chenery, S.P., 1997. A compilation of new and published major and trace element data for NIST SRM 610 and NIST SRM 612 glass reference materials. Geostandards Newsletter, 21: 115-144.

Pearce, N.J.G., Perkins, W.T., Westgate, J.A., Wade, S.C., 2011. Trace element analysis by laser ablation ICP-MS: the quest for comprehensive chemical characterisation of single sub-10um volcanic glass shards. Quaternary International, 246: 57-81.

Pearce, N.J.G., Westgate, J.A., Perkins, W.T., Preece, S.J., 2004. The application of ICP-MS methods to tephrochronological problems. Applied Geochemistry, 19: 289-322.

Peppard, D., 1969. A tetrad effect in the liquid-liquid extraction ordering of lanthanides (III). J. inorg. nucl. Chem., 31: 2271-2272.

Platz, T., Cronin, S.J., Smith, I.E.M., Turner, M.B., Stewart, R.B., 2007. Improving the reliability of microprobe-based analyses of andesitic glasses for tephra correlation. The Holocene, 17: 573-583.

Riehle, J.R., Miyaoka, R.T., Meyer, C.E., 1999. Data on Holocene tephra (volcanic ash) deposits in the Alaska Peninsula and lower Cook Inlet region of the Aleutian volcanic arc, Alaska. USGS.

Rollinson, H.R., 1993. Using Geochemical Data: Evaluation, Presentation, Interpretation. Longman Scientific and Technical Harlow, 376 pp.

Sarna-Wojcicki, A.M., Meyer, C.E., Woodward, M.J., Lamothe, P.J., 1981. Composition of air-fall ash erupted on May 18, May 25, June 12, July 22 and August 7. In: Lipman, P.W., Mullineaux,

763 D.R. (Eds.), The 1980 eruptions of Mount St. Helens, Washington. United States Geological
764 Survey Professional Paper 1250.
765 Shane, P., 2005. Towards a comprehensive distal andesitic tephrostratigraphic framework for New
766 Zealand based on eruptions from Egmont volcano. Journal of Quaternary Science, 20(1): 45-
767 57.
768 Sun, S.-s., McDonough, W.F., 1989. Chemical and isotopic systematics of oceanic basalts:
769 implications for mantle compositions and processes. In: Saunders, A.D., Norry, M.J. (Eds.),
770 Magmatism in the Ocean Basins. Geological Society Special Publication, pp. 313-345.
771 Takahashi, Y., Yoshida, H., Sato, N., Hama, K., Yusa, Y., Shimizu, H., 2002. W-and M-type tetrad
772 effects in REE patterns for water–rock systems in the Tono uranium deposit, central Japan.
773 Chemical Geology, 184(3-4): 311-335.
774 Tardy, Y., Nahon, D., 1985. Geochemistry of laterites, stability of Al-goethite, Al-hematite, and Fe3+-
775 kaolinite in bauxites and ferricretes: an approach to the mechanism of concretion formation.
776 American Journal of Science, 285(10): 865.
777 Tiedemann, R., Mix, A.C., Richter, C., Ruddiman, W.F., 2007. Proceedings of the Ocean Drilling
778 Program. Scientific Results Leg 202. , Ocean Drilling Program, College Station, Texas.
779 Todd, J.A., Austin, W.E., Abbott, P.M., 2014. Quantifying bioturbation of a simulated ash fall event.
780 In: Austin, W.E., Abbott, P.M., Davies, S.M., Pearce, N.J.G., Wastegård, S. (Eds.), Marine
781 Tepohrochronology Geological Society, London, pp. 195-207.
782 Watt, S.F., Pyle, D.M., Naranjo, J.A., Rosqvist, G., Mella, M., Mather, T.A., Moreno, H., 2011.
783 Holocene tephrochronology of the Hualaihue region (Andean southern volcanic zone,∼ 42
784 S), southern Chile. Quaternary International, 246(1-2): 324-343.
785 Weller, D., de Porras, M., Maldonado, A., Méndez, C., Stern, C., 2019. Petrology, geochemistry, and
786 correlation of tephra deposits from a large early-Holocene eruption of Mentolat volcano,
787 southern Chile. Journal of South American Earth Sciences, 90: 282-295.
788 Zhenhua, Z., Xiaolin, X., Xiaodong, H., Yixian, W., Qiang, W., Zhiwei, B., Jahn, B., 2002. Controls on
789 the REE tetrad effect in Evidence from the Qianlishan and Baerzhe granites: Granites, China.
790 Geochemical Journal, 36(6): 527-543.
791 Zimanowski, B., 2001. Phreatomagmatic explosions. In: Freundt, A., Rossi, M. (Eds.), From magma to
792 tephra: modelling physical processes of explosive volcanic eruptions. Elsevier Science,
793 Amsterdam, pp. 25-53.

794

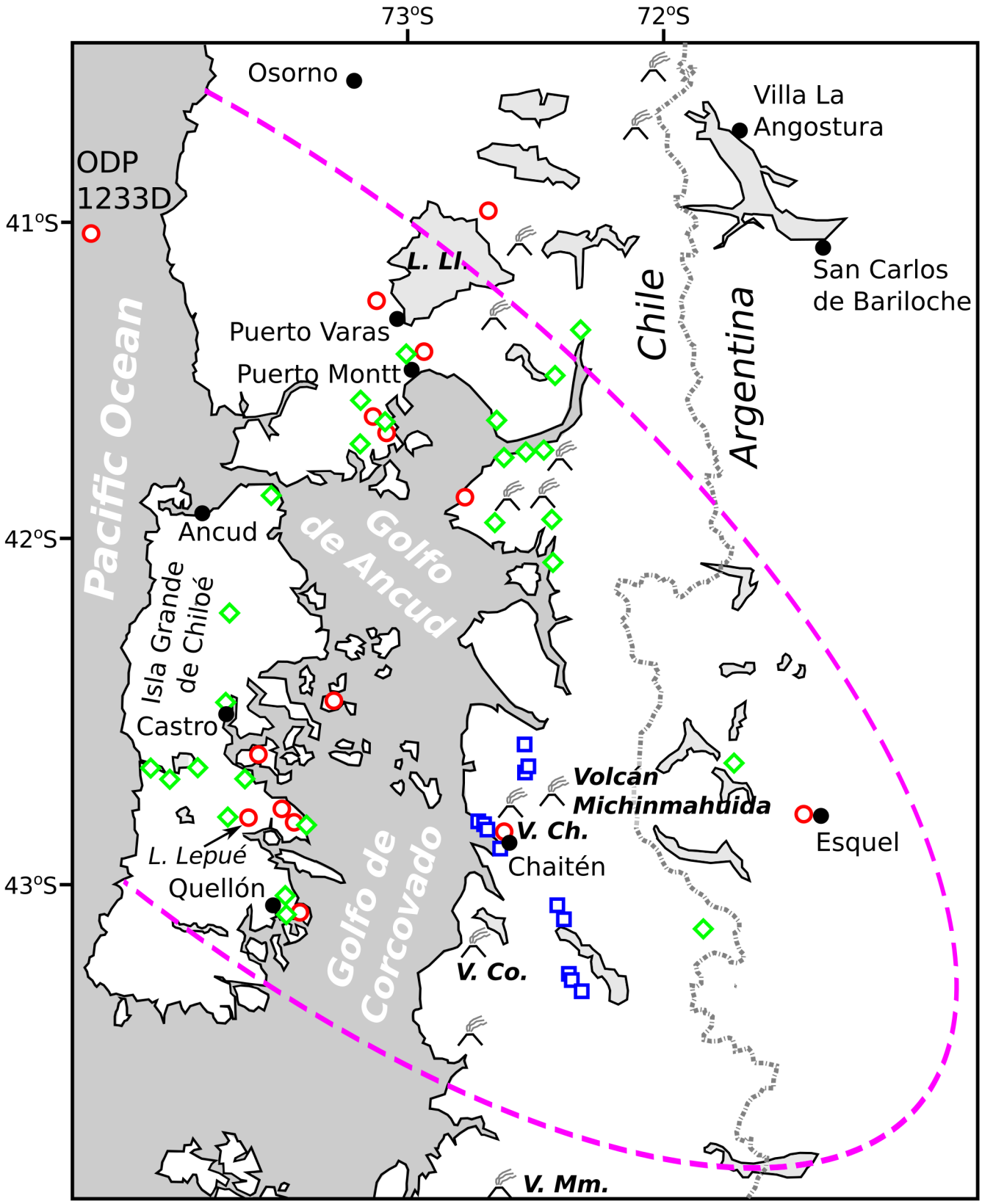
73ºS
72ºS
41ºS
42ºS
43ºS
Osorno
Villa La
Angostura
ODP
1233D
L. Ll.
San Carlos
de Bariloche
Puerto Varas
Puerto Montt
Chile
Argentina
Pacific Ocean
Ancud
Golfo
de Ancud
Isla Grande
de Chiloé
Castro
Volcán
Michinmahuida
V. Ch.
Esquel
L. Lepué
Quellón
Chaitén
Golfo de
Corcovado
V. Co.
V. Mm.

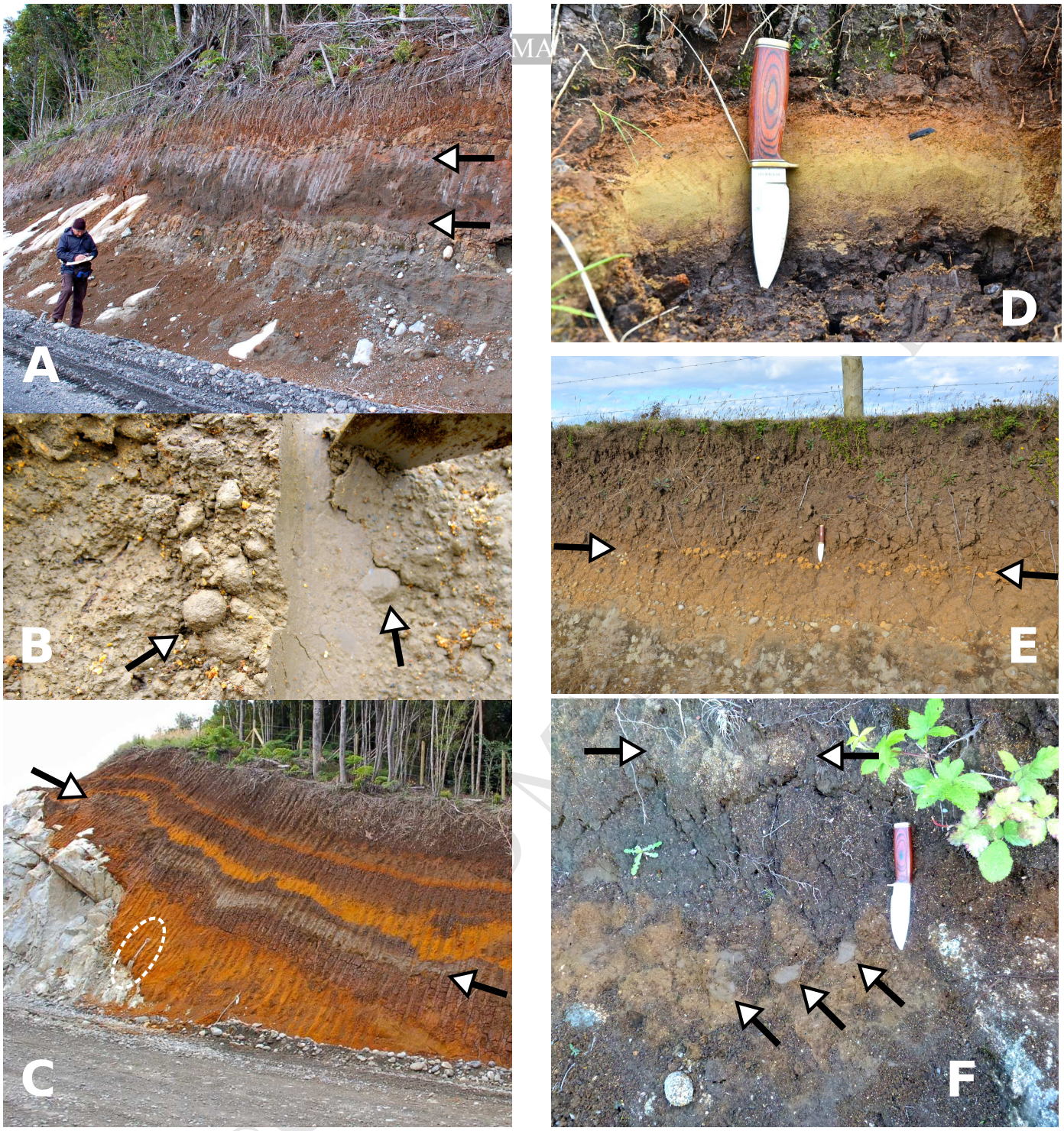
A
B
C
D
E
F

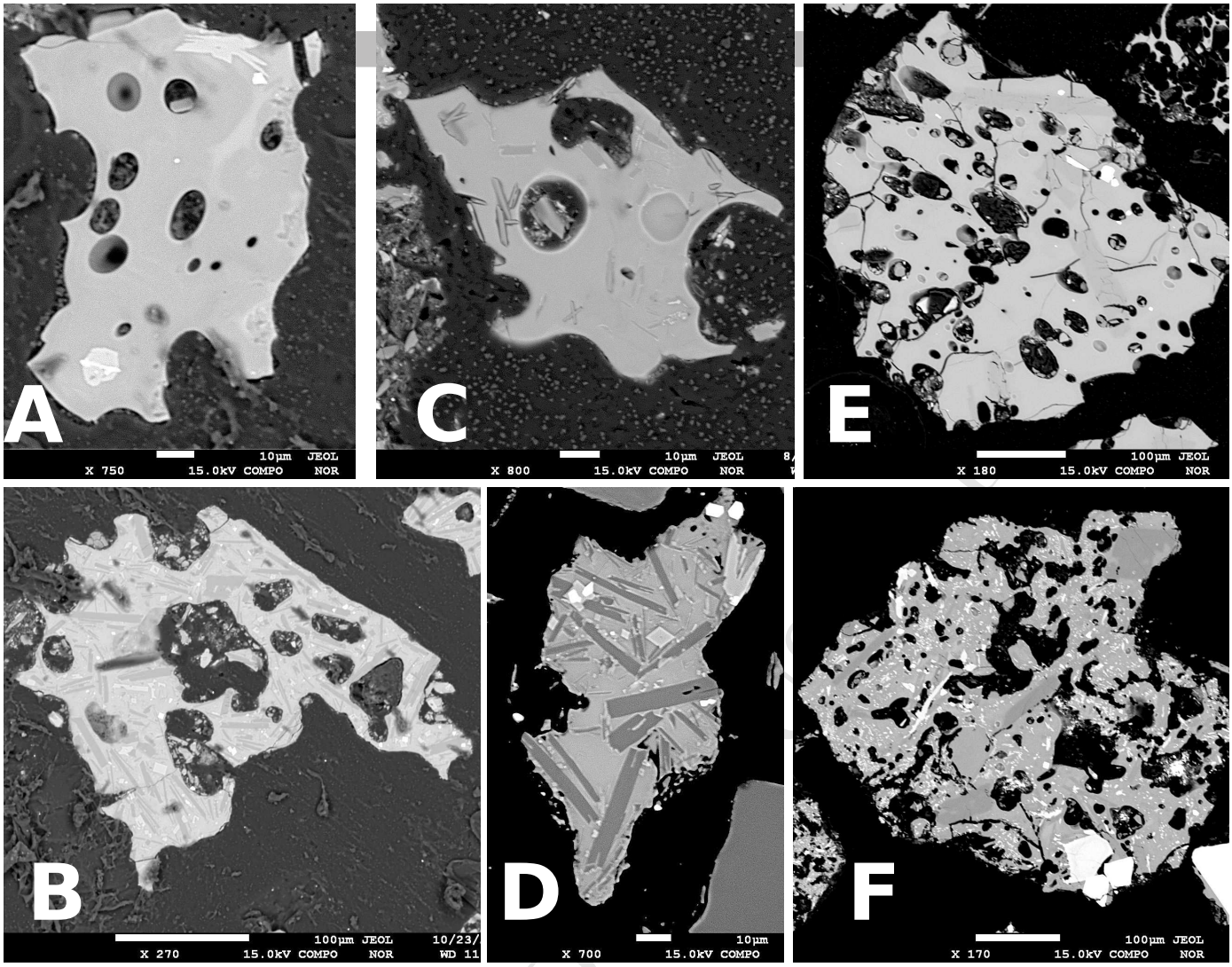
A
10µm JEOL
X 750 15.0kV COMPO NOR
C
10µm JEOL
X 800 15.0kV COMPO NOR
E
100µm JEOL
X 180 15.0kV COMPO NOR
B
100µm JEOL 10/23/
X 270 15.0kV COMPO NOR WD 11
D
10µm
X 700 15.0kV COMPO
F
100µm JEOL
X 170 15.0kV COMPO NOR